Orbital and spin ordering physics of the Mn_3O_4 spinel

Santanu Pal* and Siddhartha Lal†

Department of Physical Sciences, Indian Institute of Science Education and Research-Kolkata, Mohanpur, West Bengal 741246, India

(Received 26 April 2017; revised manuscript received 24 July 2017; published 18 August 2017)

Motivated by recent experiments, we present a comprehensive theoretical study of the geometrically frustrated strongly correlated magnetic insulator Mn_3O_4 spinel oxide based on a microscopic Hamiltonian involving lattice, spin, and orbital degrees of freedom. Possessing the physics of degenerate e_g orbitals, this system shows a strong Jahn-Teller effect at high temperatures. Further, careful attention is paid to the special nature of the superexchange physics arising from the 90° Mn-O-Mn bonding angle. The Jahn-Teller and superexchange-based orbital-spin Hamiltonians are then analyzed in order to track the dynamics of orbital and spin ordering. We find that a high-temperature structural transition results in orbital ordering the nature of which is mixed with respect to the two originally degenerate e_g orbitals. This ordering of orbitals is shown to relieve the intrinsic geometric frustration of the spins on the spinel lattice, leading to ferrimagnetic Yafet-Kittel ordering at low temperatures. Finally, we develop a model for a magnetoelastic coupling in Mn_3O_4, enabling a systematic understanding of the experimentally observed complexity in the low-temperature structural and magnetic phenomenology of this spinel. Our analysis predicts that a quantum fluctuation-driven orbital-spin liquid phase may be stabilized at low temperatures upon the application of pressure.

DOI: 10.1103/PhysRevB.96.075139

I. INTRODUCTION

Frustrated magnetic systems with orbital degeneracy present an interesting playground for the exploration of novel ordered as well as liquidlike states. Frustration leads very naturally to macroscopic degeneracy in the ground state and a concomitant lack of equilibrium spin ordering. Such spin liquid states have been proposed in theoretical studies of several systems with different types of geometrically frustrated lattices, as well as in experiments performed on some candidate materials [1–3]. It is important to note, however, that typical material systems of interest in quantum magnetism also possess orbital and lattice degrees of freedom. The interaction among these three can lead to a variety of emergent ordered states. For instance, degenerate orbital degrees of freedom interact in a cooperative manner with fluctuations of the lattice via the Jahn-Teller effect [4–6], inducing orbital ordering along with a static global distortion of the lattice. From the seminal work of Kugel and Khomskii [7,8], it is well known that strong electronic correlations give rise to superexchange (SE) related interactions between and among the orbital and spin degrees of freedom. The resultant orderings of orbitals and spins can then be strongly tied to each other. Further, the coupling of spin and lattice degrees of freedom can also be shown to have interesting consequences for spin ordering [9,10]. In this way, the presence of multiple couplings between various degrees of freedom leads generically to the separation of energy scales at which the ordering of the orbitals and spins takes place [11–14]. Equally importantly, such interactions also offer multiple ways by which the system can relieve any inherent frustration among the spins and attain their ordering.

Since orbital-spin interactions depend strongly on the metal-ligand-metal bonding angle in strongly correlated insulators [15,16], a transition-metal (TM) insulator on the geometrically frustrated spinel lattice with orbital, spin, and lattice degrees of freedom offers the exciting prospect of finding diverse physical phenomena across a wide scale of energies. In this light, the spinel Mn_3O_4 is an ideal candidate system in which the complex interplay of various spin-orbital-lattice interactions has been studied [17–23]. However, the microscopic mechanism that relieves the geometric frustration inherent in the spinel structure and leads to the ferrimagnetic Yafet-Kittel (Y-K) ordering of spins at low temperatures remains unknown [24]. Further, the SE mechanism for electronic correlations in the Mn_3O_4 spinel is likely different from the other well-studied TM perovskite systems [25,26]. In perovskite systems, where the TM-ligand-TM bond angle is 180° and the ligand site has only one orbital participating in the superexchange mechanism, one can often conclude on spin ordering by considering the nature of orbital ordering. This is the essence of the phenomenological Goodenough-Kanamori-Anderson (GKA) rules. However, in spinel systems, the 90° TM-ligand-TM bond angle necessitates two orthogonal ligand orbitals participating in superexchange. This renders inapplicable our intuition of spin ordering based on the GKA rules.

Experiments show that at 1443 K Mn_3O_4 undergoes a structural transition from cubic to tetragonal lattice symmetry [17–21,27–29]. This material also has three different magnetic transitions, with the first being a transition from a paramagnetic phase to a three-dimensional canted ferrimagnetic Yafet-Kittel spin ordering at 43 K. In the Yafet-Kittel phase, the magnetic unit cell possesses two Mn^{2+}(A-type) spins aligned along the [110] direction, together with a tetrahedra of four Mn^{3+} (B-type) spins the net moment of which is antiparallel to the Mn^{2+} spins, but with each of the four spins being canted away from the c axis ([001] direction) and towards the $[\bar{1}\bar{1}0]$ direction. This compound has further magnetic transitions at 39 and 33 K. Between these two transitions, the magnetic unit cell becomes incommensurate with respect to the chemical unit cell. Another structural transition, from tetragonal to orthorhombic lattice symmetry [20], is observed at 33 K and

*sp13rs010@iiserkol.ac.in
†slal@iiserkol.ac.in

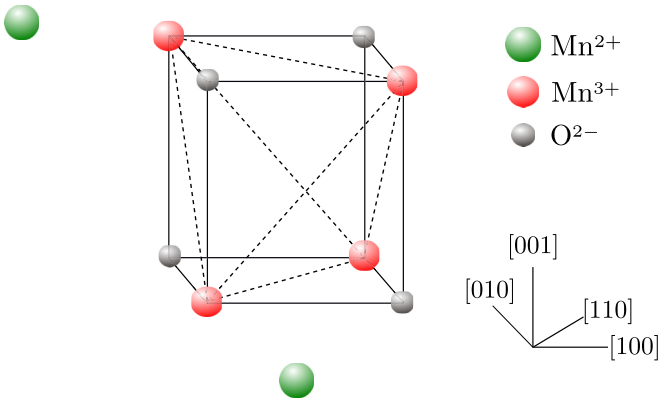

FIG. 1. Schematic diagram of a Mn_3O_4 unit cell. Four orbitally active Mn^{3+} ions (red spheres) form a tetrahedron. The Mn^{3+} ions are connected via oxygen ions (gray spheres), with the Mn-O-Mn bonding angle being 90°. There are also two orbitally nonactive Mn^{2+} ions (green spheres) present in the unit cell.

the Yafet-Kittel magnetic order is again attained, but with a unit cell doubled along the [110] direction with respect to the ordered phase at 43 K. Experiments also show that the magnetic transitions are associated with a significant change in the in-plane (electric field $\vec{E} \parallel [100]$) and out-of-plane ($\vec{E} \parallel [001]$) components of the dielectric constant, indicating a strong spin-lattice coupling [19,21,22,30].

In this paper, we attempt a qualitative understanding of underlying physics of ordering in the Mn_3O_4 spinel by the development of a microscopic model for the orbital, spin, and lattice degrees of freedom. Keeping in mind the special 90° TM atom-ligand atom-TM atom bonding angle in Mn_3O_4 (a typical Mn^{3+} tetrahedra is shown in Fig. 1), we carry out a systematic derivation of the orbital-spin Hamiltonian. We then perform a variational analysis of this Hamiltonian to find the nature of orbital ordering at higher-energy scales and resultant spin ordering at lower energies. In understanding the low-temperature structural transition (tetragonal to orthorhombic) and associated magnetic and orbital orders, we also develop a model for the spin-lattice interaction in this system.

This paper is organized as follows. In Sec. II, we derive the orbital-spin model. In Sec. III, we analyze this Hamiltonian and discuss our results for orbital ordering. Using the orbital order found in Sec. III, we then compute the magnetic interaction in different crystallographic planes in Sec. IV, along with a discussion of spin ordering at low temperatures. In Sec. V, we develop a model for the spin-lattice interaction and relate our results to explain some experimental facts. We end with a concluding section.

II. SPIN-ORBITAL HAMILTONIAN

The Mn_3O_4 spin-orbital model is based on the spinel lattice, where nearest-neighbor transition-metal ions are connected via oxygen ligand atoms with an ion-oxygen-ion bond angle of 90°. Due to the presence of a crystal field, the $3d$ electron levels of the Mn^{3+} ion split into t_{2g} and e_g levels [22]. Further, for an on-site Hubbard repulsion on the transition-metal ion that is much greater than the crystal-field splitting, the Mn^{3+} ion's four d electrons form a high-spin configuration

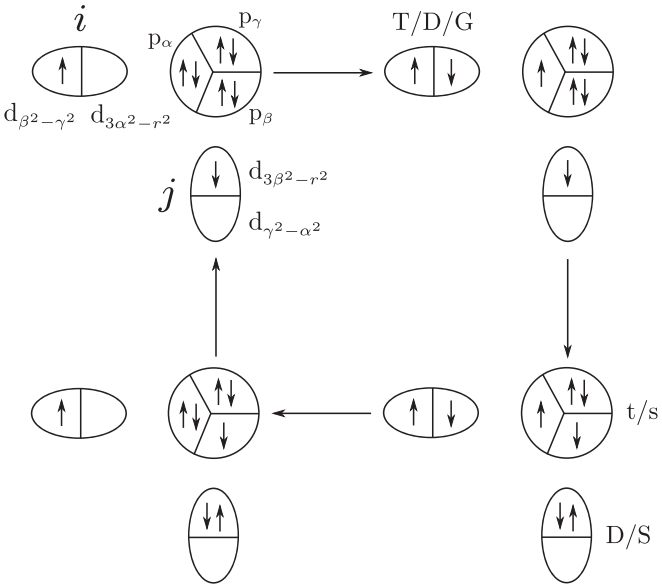

FIG. 2. Four-step SE process for a M-type initial configuration (following notations of [16]). An oval represents the Mn^{3+} ion with one e_g electron either in the nonhopping orbital ($d_{\beta^2-\gamma^2}$) on the left or in the hopping orbital ($d_{3\alpha^2-r^2}$) on the right. A circle represents an oxygen ion with the electrons in the p orbitals. T, D, G, and S are excited states of the Mn^{3+} ion. The triplet t and singlet s are excited-state configurations of the oxygen ion. Note that $\{\alpha,\beta,\gamma\}$ is a cyclic permutation of $\{x,y,z\}$.

with spin $S = 2$ [31]. As shown by Mostovoy and Khomskii [15] and Reitsma *et al.* [16] for the case of a 90° TM-O-TM bond angle, the Anderson superexchange process (where an electron is effectively transferred from one metal ion site to the other metal ion site) is considerably weaker than the Goodenough superexchange process (where two electrons transfer from the ligand oxygen ion, one to each of the neighbor metal ions). The Goodenough superexchange process is schematically represented as

$$e^1 p^6 e^1 \rightarrow e^1 p^5 e^2 \rightarrow e^2 p^4 e^2 \rightarrow e^1 p^5 e^2 \rightarrow e^1 p^6 e^1, \quad (1)$$

where e and p represent the e_g orbital on the transition metal (Mn^{3+}) and p orbital on the ligand (O) sites, respectively. The effective spin-orbital Hamiltonian is obtained from fourth-order perturbation theory. As shown in Fig. 2, in the excitation process of the SE mechanism, one electron hops from a p_α orbital of the ligand oxygen atom to the left Mn^{3+} ion e_g orbital, while another electron hops from a p_β orbital of the same oxygen atom to the down Mn^{3+} ion orbital. In the de-excitation process, excited electrons return to the oxygen atom by reversing the hopping pathway. In this way, correlations build between the two Mn^{3+} ions and contribute to the SE. The relevant Mn^{3+} e_g states are ${}^4A_2$, ${}^4E$, ${}^4A_1$, and ${}^6A_1$. Of these, the first is a singlet (S), the second and third are Hund's-split orbital doublets (D, G), and the fourth is a triplet (T), with energy $E_S = U + \frac{10}{3}J_H$, $E_D = U + \frac{2}{3}J_H$, $E_G = U$, and $E_T = U - 5J_H$ [31,32], respectively. The oxygen p^4 configurations that occur during the SE process include a triplet ${}^3T_1$ (t) and singlet ${}^1T_2$ (s) with energy $U_p - J_p$ and $U_p + J_p$, respectively. Here U, J_H and U_p, J_p are the interorbital

Coulomb repulsion and Hund's exchange couplings on the Mn^{3+} and oxygen ion sites, respectively. In deriving the complete spin-orbital Hamiltonian, we follow the formulation and notations of Ref. [16]. While the detailed derivation is presented in the Appendix, we present here the results. It should be noted that, in reaching the spin-orbital Hamiltonian, one must list all possible initial configurations (the electron's position on the hopping or nonhopping orbital of Mn sites), and for each of them list all possible hopping sequences that return to the ground-state manifold. Thus, the spin-orbital Hamiltonian we begin with has the form

$$\mathcal{H}_{\rm eff} = \sum_{\langle ij\rangle,\alpha\neq\beta} \big(\mathcal{Q}^{\alpha\beta}_{O,ij}\big[K^T_O \mathcal{Q}^T_{ij} + K^S_O \mathcal{Q}^S_{ij}\big] + \mathcal{Q}^{\alpha\beta}_{M,ij}\big[K^T_M \mathcal{Q}^T_{ij} + K^S_M \mathcal{Q}^S_{ij}\big] + \mathcal{Q}^{\alpha\beta}_{N,ij}\big[K^T_N \mathcal{Q}^T_{ij} + K^S_N \mathcal{Q}^S_{ij}\big]\big) \quad (2)$$

where $\mathcal{Q}$ are the orbital projection operators denoted by

$$\begin{aligned}
\mathcal{Q}^{\alpha\beta}_{O,ij} &= \mathcal{P}^{\alpha}_i \mathcal{P}^{\beta}_j + \mathcal{P}^{\beta}_i \mathcal{P}^{\alpha}_j,\\
\mathcal{Q}^{\alpha\beta}_{M,ij} &= \mathcal{P}^{\alpha}_i \mathcal{P}^{\bar\beta}_j + \mathcal{P}^{\bar\alpha}_i \mathcal{P}^{\beta}_j + \mathcal{P}^{\beta}_i \mathcal{P}^{\bar\alpha}_j + \mathcal{P}^{\bar\beta}_i \mathcal{P}^{\alpha}_j,\\
\mathcal{Q}^{\alpha\beta}_{N,ij} &= \mathcal{P}^{\bar\alpha}_i \mathcal{P}^{\bar\beta}_j + \mathcal{P}^{\bar\beta}_i \mathcal{P}^{\bar\alpha}_j,
\end{aligned} \quad (3)$$

where $\alpha,\beta \in \{x,y,z\}$, $\mathcal{P}^{\alpha}_i = (\frac{1}{2}\mathbf{I}_i + I^{\alpha}_i)$, and $\mathcal{P}^{\bar\alpha}_i = (\frac{1}{2}\mathbf{I}_i - I^{\alpha}_i)$ are projection operators for the hopping and nonhopping orbitals, respectively, and $\mathbf{I}$ is the 2×2 identity matrix. The (rotated) orbital pseudospin operators (I) are given by

$$I^{x/y}_i = -\frac{1}{2}T^z_i \mp \frac{\sqrt{3}}{2}T^x_i, \quad I^z_i = T^z_i, \quad (4)$$

where T represents the pseudospin operators for the twofold degenerate e_g orbital system, with the orbital Hilbert space at each site given by

$$\begin{pmatrix}1\\0\end{pmatrix} = |3z^2 - r^2\rangle, \quad \begin{pmatrix}0\\1\end{pmatrix} = |x^2 - y^2\rangle. \quad (5)$$

The orbital projection operators determine the precise configuration of the orbitals on any two Mn^{3+} ions connected by a hopping pathway, e.g., whether both hopping orbitals are occupied by an electron each (denoted by "O"), any one of the two hopping orbitals occupied (denoted by "M"), and neither hopping orbital occupied (denoted by "N"). Further, Q are spin projection operators denoted by

$$Q^T_{ij} = \tfrac{1}{10}(6 + \vec{S}_i.\vec{S}_j), \quad Q^S_{ij} = \tfrac{1}{10}(4 - \vec{S}_i.\vec{S}_j), \quad (6)$$

where T stands for triplet and S for singlet spin configurations at Mn sites. Finally, the Ks are various spin-orbital SE constants.

The Hamiltonian may be separated into purely orbital ($\mathcal{O}$) and spin-orbital ($\mathcal{S}$) parts as follows:

$$\mathcal{H}_{\rm eff} = \sum_{\langle ij\rangle,\alpha\neq\beta} \big(\big[J^{\mathcal{O}}_O \mathcal{Q}^{\alpha\beta}_{O,ij} + J^{\mathcal{O}}_M \mathcal{Q}^{\alpha\beta}_{M,ij} + J^{\mathcal{O}}_N \mathcal{Q}^{\alpha\beta}_{N,ij}\big]\mathbf{1}_{ij} + \big[J^{\mathcal{S}}_O \mathcal{Q}^{\alpha\beta}_{O,ij} + J^{\mathcal{S}}_M \mathcal{Q}^{\alpha\beta}_{M,ij} + J^{\mathcal{S}}_N \mathcal{Q}^{\alpha\beta}_{N,ij}\big]\vec{S}_i.\vec{S}_j\big), \quad (7)$$

with interorbital and spin-orbital interaction constants given by

$$\begin{aligned}
J^{\mathcal{O}}_L &= \tfrac{1}{10}\big(6K^T_L + 4K^S_L\big),\\
J^{\mathcal{S}}_L &= \tfrac{1}{10}\big(K^T_L - K^S_L\big)(L = O,M,N).
\end{aligned} \quad (8)$$

In order to calculate the SE constant, one has to consider closely the four-step SE process. As an example, consider the M initial configuration $|M,\uparrow\downarrow\rangle$ (as shown in Fig. 2). Here, a single electron (with spin-up) occupies a nonhopping orbital ($d_{\beta^2-\gamma^2}$) on the ith site of Mn^{3+}, while another electron (with spin-down) occupies the hopping orbital ($d_{3\beta^2-r^2}$) on the jth site. The corresponding contribution to the SE coupling is denoted by $[M,\uparrow\downarrow;\downarrow\uparrow]$, where the final ($\downarrow\uparrow$) denotes the configuration of hopping electrons from the oxygen sites. As we will see below, $[M,\uparrow\downarrow;\downarrow\uparrow]$ involves contributions from 12 possible doubly excited states denoted succinctly by $[XvY]$, with $X,Y \in \{T,D,S,G\}$ and $v \in \{t,s\}$:

$$\begin{aligned}
[M,\uparrow\downarrow;\downarrow\uparrow] = \tfrac{1}{3}([TtD] + [TtS] + [DtD] + [DtS]\\
+ [TsD] + [TsS] + [DsD] + [DsS]\\
+ [GtD] + [GtS] + [GsD] + [GsS]),
\end{aligned} \quad (9)$$

with

$$[XvY] = \frac{t^4}{4}\frac{\Delta_X + \Delta_Y}{\Delta^2_X \Delta^2_Y}\frac{U_v}{\Delta_X + \Delta_Y + U_v}, \quad (10)$$

where $U_s = U_p + J_p$, $U_t = U_p - J_p$, $\Delta_T = \Delta - 4J_H$, $\Delta_D = \Delta + \frac{5}{3}J_H$, $\Delta_S = \Delta + \frac{13}{3}J_H$, $\Delta_G = \Delta + J_H$, and $\Delta = U - J_H$. Here t is the charge-transfer amplitude. The factor $1/3$ takes care of the threefold processes arising from the T, D, and G spin configurations of an excited state (see Fig. 2). Note that we have four sequences of excitation and de-excitation processes for a given intermediate doubly excited state. The other "M" configurations as well as "O" and "N" configurations are taken account of in a similar manner (see the Appendix for more details).

The complete spin-orbital Hamiltonian can then be written in a compact notation as follows:

$$\mathcal{H}_{\rm eff} = \sum_{\langle ij\rangle,\alpha\neq\beta} J_\tau \mathcal{W}^{\alpha\beta}_{ij} + \sum_{\langle ij\rangle,\alpha\neq\beta} \big(-J_\sigma \mathbf{1}_{ij} + J_\nu \mathcal{V}^{\alpha\beta}_{ij} - J_\mu \mathcal{W}^{\alpha\beta}_{ij}\big)\vec{S}_i.\vec{S}_j, \quad (11)$$

where $\mathcal{V}^{\alpha\beta}_{ij} = -\mathbf{1}_i(I^{\alpha}_j + I^{\beta}_j) - (I^{\alpha}_i + I^{\beta}_i)\mathbf{1}_j$ and $\mathcal{W}^{\alpha\beta}_{ij} = 2(I^{\alpha}_i I^{\beta}_j + I^{\beta}_i I^{\alpha}_j)$. The first term denotes interorbital interactions and the second term denotes spin-orbital interactions. The algebraic expression of the various SE constants (J_τ, J_σ, J_ν, and J_μ) are presented in the Appendix. It is also worth noting that the form of the interorbital SE Hamiltonian and the Jahn-Teller Hamiltonian derived from phonon-orbital interactions for the spinel lattice [33] are the same.

For an idea of the relative magnitude of various SE constants in the Mn_3O_4 spinel model Hamiltonian, we have plotted them in units of t^4/Δ^3 versus U_p/Δ, where U_p is treated as a free parameter (see Fig. 3). We have also taken values for several other parameters from the existing literature. This includes Hund's coupling on the Mn^{3+} site ($J_H = 0.69$ eV), the charge-transfer transfer energy ($\Delta = 5.5$ eV), Hubbard repulsion on the TM site ($U = \Delta + J_H = 6.19$ eV) [31,34], and Hund's coupling on the oxygen site ($J_p = 0.1U_p$) [16]. It is important to note from Fig. 3 that, among all these SE couplings, only J_ν

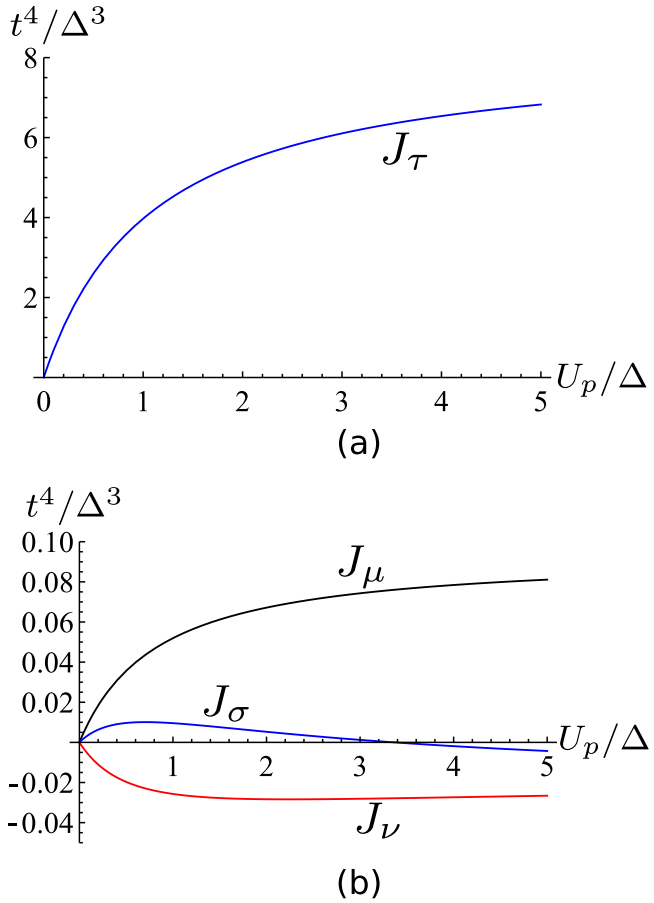

FIG. 3. A plot of various SE interaction constants (in units of $J = t^4/\Delta^3$) as a function of U_p/Δ for $J_p/U_p = 0.1$ and $J_H/\Delta = 0.14$: (a) orbital SE constant J_τ and (b) spin-orbital SE constants J_μ, J_ν, and J_σ. Estimates of some of the parameters for Mn_3O_4 taken from the literature are $U_p/\Delta = 0.909$, $J_H = 0.69$ eV, and $\Delta = U - J_H = 5.5$ eV [16,31,35,36].

is negative for the Mn_3O_4 spinel. Further, it is also clear that the interorbital interaction J_τ is much greater than all spin-orbital interactions. Thus, orbital ordering must dominate the physics of this Hamiltonian at high-energy scales.

III. VARIATIONAL ANALYSIS OF THE INTERORBITAL HAMILTONIAN

Recalling the fact that among different SE constants the interorbital SE term (J_τ) dominates over all other exchange terms (see Fig. 3), we analyze the interorbital part of the Hamiltonian first in order to obtain the orbital ordering that will set in at high-energy scales. The form of the interorbital mean field Hamiltonian is given by

$$\mathcal{H}_{\rm MF} = \sum_{\langle i,j\rangle,\alpha\neq\beta} J_\tau \langle \mathcal{W}_{ij}^{\alpha\beta}\rangle. \tag{12}$$

We use a general superposition of the orbital basis state for a variational analysis

$$|\theta_i\rangle = \cos(\theta_i/2)|3z^2 - r^2\rangle + \sin(\theta_i/2)|x^2 - y^2\rangle, \tag{13}$$

such that the expectation value of the orbital operator $\mathcal{W}_{ij}$ acting on the direct-product orbital state specifying the bond lying between the ith and jth sites, $|\theta_i\rangle \otimes |\theta_j\rangle$, is obtained as

$$\begin{aligned}\langle \mathcal{W}_{ij}^{\alpha\beta}\rangle = {} & \frac{1}{4}[2\cos(\theta_i+\theta_j) - \cos(\theta_i-\theta_j)]_{xy} \\ & + \frac{1}{4}\left[2\cos\left(\theta_i+\theta_j-\frac{4\pi}{3}\right) - \cos(\theta_i-\theta_j)\right]_{xz} \\ & + \frac{1}{4}\left[2\cos\left(\theta_i+\theta_j+\frac{4\pi}{3}\right) - \cos(\theta_i-\theta_j)\right]_{yz}.\end{aligned} \tag{14}$$

Here, the suffix at the end of each bracket indicates the plane on which the particular Mn-O-Mn bond lies within a given Mn^{3+} tetrahedron. Note that we assume a vanishing relative phase between the two e_g orbitals in Eq. (13) above due to the presence of time-reversal invariance [37,38].

It can be shown that, for the case of 90° bonding between the transition-metal ions, a ferro-orbital (FO) configuration ($\theta_i \simeq \theta_j$) is favored energetically over a canted-orbital (CO) configuration ($\theta_i \simeq \theta_j \pm \pi$) [8,16]. Considering these subtleties in our analysis, we compute the variational ground-state orbital ordering for the Mn_3O_4 spinel. The variational energy for this FO configuration of a tetragonally distorted spinel (the lattice length scale along the c axis is greater than that along the a and b axes, $c > a = b$) is found to be

$$E(\theta) = \frac{J_\tau}{4}[2(1-\beta)\cos 2\theta - (1+2\beta)], \tag{15}$$

where the XY-plane SE constant is given by $J_\tau^{ab} = J_\tau$, and the XZ- and YZ-plane constants are given by $J_\tau^{ac} = J_\tau^{bc} = \beta J_\tau$, $\beta < 1$. Then, minimizing $E(\theta)$ gives

$$\frac{\partial E(\theta)}{\partial\theta} = -J_\tau(1-\beta)\sin 2\theta,$$
$$\frac{\partial^2 E(\theta)}{\partial\theta^2} = -2J_\tau(1-\beta)\cos 2\theta,$$

such that, for $\beta < 1$, $E(\theta)$ will have minima at $\theta = \pm(2n+1)\pi/2$ (where n is integer). For $\theta = \pm\pi/2$, the so-called mixed orbital ordering states are given by [13,16,38–40] $|\theta = \pm\frac{\pi}{2}\rangle = \frac{1}{\sqrt{2}}|3z^2 - r^2\rangle \pm \frac{1}{\sqrt{2}}|x^2 - y^2\rangle$. This orbital ordering has a twofold degeneracy shown in Fig. 4, reflecting the $a = b$ axes symmetry of the tetragonally distorted spinel.

A. Computation of spin-exchange couplings

The spin-orbital Hamiltonian (11) shows that the dynamics of the orbitals and spin degrees of freedom are coupled to one other. Thus, orbital ordering at high temperatures must dictate low-temperature spin ordering. Thus, once orbital ordering is obtained variationally, one can use the orbital-ordering angle $\theta = \pm\pi/2$ in the spin-orbital Hamiltonian in deriving an effective spin-exchange interaction between spins in different crystallographic directions. In this way, along the three crystallographic planes (XY, XZ, and YZ), the effective

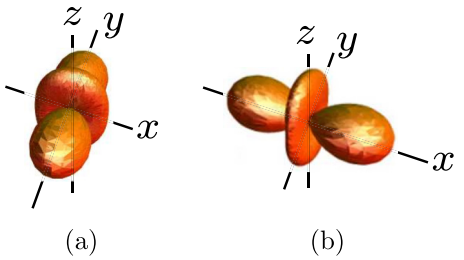

FIG. 4. The mixed orbital state for (a) orbital angle $\theta = +\pi/2$ and (b) orbital angle $\theta = -\pi/2$.

spin Hamiltonian has the form [upon neglecting the small J_σ term in Eq. (11)]

$$H_{xy}^{\rm spin}(\theta = \pm\pi/2) = 0.75 J_\mu \vec{S}_i.\vec{S}_j = J_{BB}\vec{S}_i.\vec{S}_j,$$
$$H_{xz}^{\rm spin}(\theta = \pm\pi/2) = \pm 0.865\bar{\alpha}|J_\nu|\vec{S}_i.\vec{S}_j = \pm J'_{BB}\vec{S}_i.\vec{S}_j,$$
$$H_{yz}^{\rm spin}(\theta = \pm\pi/2) = \mp 0.865\bar{\alpha}|J_\nu|\vec{S}_i.\vec{S}_j = \mp J'_{BB}\vec{S}_i.\vec{S}_j. \quad (16)$$

In obtaining Eqs. (16), we have used the expression for the expectation values of the orbital operators $\mathcal{W}_{ij}$ [Eq. (14)] and $\langle \mathcal{V}_{ij}^{\alpha\beta}\rangle = \cos[(\theta_i+\theta_j)/2+\chi_\gamma]\cos[(\theta_i-\theta_j)/2]$, where $\chi_\gamma = 4\pi/3, -4\pi/3$ and 0 for $\gamma = x,y,z$, respectively, and $\{\alpha,\beta,\gamma\}$ is a cyclic permutation of $\{x,y,z\}$. For a system with tetragonal symmetry, the ratio of superexchange-based spin-exchange couplings $\bar{\alpha}(\equiv J_\nu^{xz}(J_\nu^{yz})/J_\nu^{xy}) < 1$. Our results show that the antiferromagnetic spin exchange between the B-type moments (i.e., Mn^{3+} ions) in the XY planes is given by $J_{BB} = 0.75 J_\mu$. However, the exchange coupling between B-type moments in the other planes is considerably weaker in value, $J'_{BB} = 0.865\bar{\alpha}|J_\nu| \ll J_{BB}$, and can be either ferromagnetic or antiferromagnetic depending on the sign of the orbital angle θ. As a result, the geometrical frustration inherent in a Mn^{3+} tetrahedron is relieved by the mixed nature of the orbital-ordered ground state.

We can also obtain numerical estimates of the spin SE constants derived from our model. For this, we use the ratios $J_\tau/J_\mu \sim 60$ and $J_\tau/J_\nu \sim 140$ obtained from Fig. 3 for the Mn_3O_4 system ($U_p/\Delta = 0.91$). Thus, for $J_\tau \sim 1500$ K, $J_\mu \sim 25$ K and we obtain $J_{BB} = 18.75$ K from Eq. (16). Further, by considering an anisotropy factor $\bar{\alpha} = 0.5$, we also obtain $J'_{BB} = 4.75$ K from Eq. (16). We note that the values obtained for both J_{BB} and J'_{BB} are in reasonable agreement with those found from experiments and first-principles calculations [24,41].

B. Spin ordering in the Mn_3O_4 spinel

While the Mn_3O_4 spinel system undergoes a structural phase transition from cubic to tetragonal (and consequent orbital ordering) at 1400 K, spin ordering happens only at around 42 K. The reason for a lack of spin ordering in a temperature range as large as $42 < T < 1400$ K is indicated by the low values of the various spin-exchange constants with respect to the interorbital coupling (J_τ). The largest of these

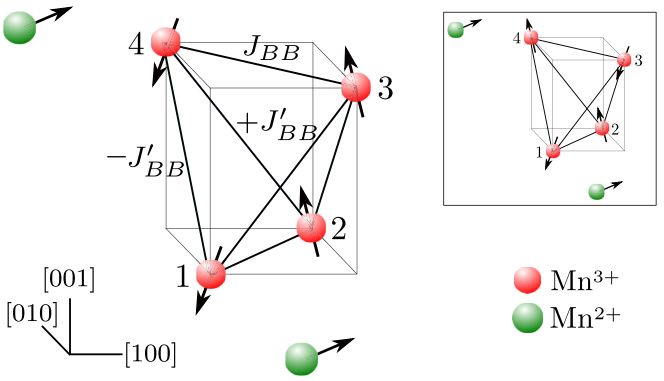

FIG. 5. Schematic diagram of a Yafet-Kittel ferrimagnetic spin configuration in the Mn_3O_4 spinel. Two Mn^{2+} spins align ferromagnetically along the [110] direction whereas four Mn^{3+} spins cant toward the $[\bar{1}\bar{1}0]$ direction with a resultant moment along $[\bar{1}\bar{1}0]$. The inset shows another Yafet-Kittel configuration which is degenerate with that shown in the main figure.

spin-exchange couplings, $J_{BB} > 0$, leads to the formation of one-dimensional (1D) antiferromagnetic spin chains in the [110] and $[1\bar{1}0]$ directions in this temperature range. While the Mn^{3+} spins are $S = 2$, the large on-site Hund's coupling ensures that only the $S^z = \pm 2$ is manifest in the dynamics. In effect, we can treat the spins as effectively spin-1/2, with any 1D chain having two degenerate classical Neél-type ground-state configurations. As is well known, such 1D spin chains cannot display any true long-ranged ordering of spins at any finite temperature; at best, a quasi-long-ranged (or algebraic) order is obtained [42]. Thus, a true long-ranged spin ordering can only be obtained at low temperatures through weaker spin-exchange couplings, including the antiferromagnetic Mn^{3+}-Mn^{2+} coupling (J_{AB}) and the interchain spin-exchange couplings J'_{BB} (some of which are ferromagnetic, and some antiferromagnetic, in nature) [24,41].

In order to understand the appearance of the ferrimagnetic Yafet-Kittel long-ranged spin order at low temperatures, we will consider the competing interactions within a single Mn-ion complex of two Mn^{2+} spins and a tetrahedron of four Mn^{3+} spins. The canting of the Mn^{3+} spins in the Y-K state can be seen to arise from having to satisfy the weak antiferromagnetic Mn^{3+}-Mn^{2+} coupling (J_{AB}) together with the in-chain Neél order due to J_{BB}. The yet weaker spin-exchange couplings J'_{BB} and J_{AA} help relieve the frustration and stabilize the Y-K ground state [43–46]. Note that the antiferromagnetic nature of J_{AB}, together with the canting of the Mn^{3+} spins, will lead to a ferrimagnetic ground state: the four Mn^{3+} spins will possess a total magnetic moment smaller than, and antialigned with, the two Mn^{2+} spins. As the system has tetragonal ($a = b$) symmetry as well as orbital degeneracy, the Y-K spin ordering is doubly degenerate (see Fig. 5). It is also known that an orthorhombic structural distortion finally stabilizes magnetic and orbital ordering in the system at around 32 K. Thus, in the next section, we show how a spin-lattice coupling lifts the spin degeneracy via an orthorhombic distortion of the Mn^{3+} tetrahedra [10,21,22], attaining a cell-doubled Y-K spin-ordered ground state.

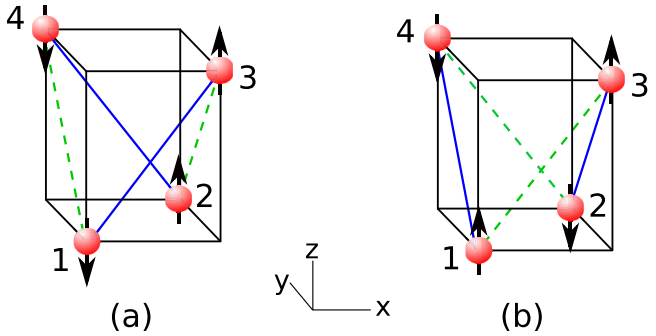

FIG. 6. The two orthorhombic forces given in Eq. (19). Dashed lines correspond to the repulsive forces between spins and the resultant elongation of the plane on which they are lying, while solid lines correspond to attractive forces and resultant compression of the plane. (a) This configuration supports elongation along the y axis while (b) supports elongation along the x axis.

IV. SPIN-LATTICE INTERACTION IN THE SPINEL

Although the geometrical frustration of the spinel lattice is relieved by the tetragonal distortion, a twofold degeneracy remains in the choice of the nature of the exchange interactions between spins in the XZ and YZ planes, J'_{BB}, in a given tetrahedron. This can be observed in Eq. (16) above. As shown in Fig. 6 below, these two degenerate configurations are associated with different orthorhombic ($a \neq b$) lattice distortions of the system [21]. Studies of the effects of a spin-lattice coupling in spinel [47,48] and pyrochlore [10] systems show how magnetic ordering can be achieved via orthorhombic distortions. In seeking the eventual stabilization of magnetic order in orthorhombically distorted Mn_3O_4, we follow an analysis similar to Ref. [10].

Allowing for a dependence of the SE constant J_{ij} on the distance between spins at sites i and j, the contribution of such a pair to the exchange energy [9,49,50] is given by

$$E_{ij} = [J + (dJ/dr)\delta r_{ij} + \cdots](\vec{S}_i \cdot \vec{S}_j). \tag{17}$$

Therefore, the spins exert on each other a force, $-(dJ/dr)(\vec{S}_i \cdot \vec{S}_j)$, which is attractive or repulsive depending on the angle between the two spins. In general, the angles between the nearest-neighbor spins placed at the vertices of a lattice can be unequal. This leads naturally to an unbalanced force acting on each spin, cooperatively resulting in a deformation of the lattice. Such a spin-lattice coupling has been called the "spin-Teller" interaction [48,49], the form of which is taken to be [51]

$$\mathcal{H}_{\rm SL} = \sum_{i,j} (\partial J_{ij}/\partial r)(\vec{S}_i \cdot \vec{S}_j)\delta r_{ij}, \tag{18}$$

where δr_{ij} is the elongation along the one axis (a or b), and $\partial J_{ij}/\partial r$ is itself a negative quantity.

Due to interorbital interactions, tetrahedra of Mn^{3+} spins are already tetragonally distorted (i.e., have a reduced symmetry, $c > a = b$). From the spin-orbital Hamiltonian, we know that the spin-exchange couplings in the XY planes are strong and antiferromagnetic. This makes it plausible that, among all possible phonon modes for a tetrahedron, a weak spin-lattice coupling will likely lead to an orthorhombic distortion. The

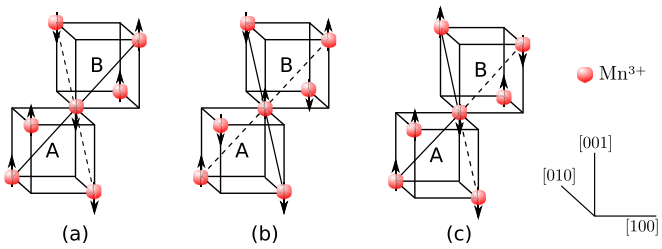

FIG. 7. Two nearest-neighbor tetrahedra A and B in a spinel lattice with their respective orientations of the Mn^{3+} ions. In all three configurations, the XY plane interaction is strong and antiferromagnetic. The spin-lattice coupling leads to an overall distortion along the [010] direction (a), along the [100] direction (b), and along the [110] direction (c), leading to a cell-doubled Yafet-Kittel spin state.

form of the orthorhombic force is given by [49]

$$f = (\vec{S}_1 - \vec{S}_2)\cdot(\vec{S}_3 - \vec{S}_4)/2 \quad \text{or} \quad (\vec{S}_1 - \vec{S}_2)\cdot(\vec{S}_4 - \vec{S}_3)/2, \tag{19}$$

where the distortion corresponding to the first term is shown in Fig. 6(a) and that corresponding to the second term is shown in Fig. 6(b). The energy of the system then has the form

$$E = -J' f \cdot \delta r + k\delta r^2/2, \tag{20}$$

where δr is the amplitude of orthorhombic distortion and J' ($= \partial J/\partial r$) and k are the magnetoelastic and elastic constants, respectively.

Now to consider the collective orthorhombic distortion ($q = 0$), we have to take into account the fact that the relevant degree of freedom arises from the existence of two different types of tetrahedra in a spinel, namely, A and B (as shown in Fig. 7), that differ in their orientation. At linear order in the displacements, there are only two active modes which couple to the spins—E_g(acoustic mode, overall orthorhombic distortion) and E_u (optical mode, tetrahedrons distorted in exactly opposite direction). These two modes can be expressed in terms of the scalar quantities

$$Q^g = \frac{Q^A + Q^B}{\sqrt{2}}, \quad Q^u = \frac{Q^A - Q^B}{\sqrt{2}}. \tag{21}$$

The spin-lattice energy is then

$$E(f^A, f^B, Q^A, Q^B) = J'(Q^A.f^A + Q^B.f^B) + \frac{k_g}{2}|Q^g|^2 + \frac{k_u}{2}|Q^u|^2. \tag{22}$$

The minimization of this energy with respect to the two lattice modes Q^g and Q^u gives

$$E(f^A, f^B) = -\frac{(K_g + K_u)(|f^A|^2 + |f^B|^2)}{4} - \frac{K_g - K_u}{2} f^A.f^B, \tag{23}$$

where $K_{g/u} = J'^2/k_{g/u}$ are the effective spin-lattice coupling constants. The first term in the expression of the energy is the self-interaction term for individual tetrahedra, and the second term is the interaction term between tetrahedra.

In the limit $K_g > K_u$ (i.e., the E_g mode softens first), the distortions of the two tetrahedra have the same nature, i.e., in order to minimize energy, f^A and f^B have to support a distortion along the same axis [see Figs. 7(a) and 7(b)]. However, in the limit $K_u > K_g$ (i.e., the E_u mode softens first), the two tetrahedra distort in an equal and opposite manner, i.e., f^A and f^B elongate along the x and y axis, respectively (see Fig. 6). Clearly, this case leads to a doubling of the magnetic unit cell, as observed in various experiments on Mn_3O_4 [19–22,28]. There remains one subtlety worth discussing. We recall that our analysis yielded two degenerate configurations of the orbitals (characterized by the mixing angle $\theta = \pm\pi/2$) in the tetrahedral phase. This immediately leads to two degenerate possible cell-doubled structures: each of the two sublattices can have an orbital state with either $\theta = \pi/2$ or $-\pi/2$, with an alternation leading to the doubling of the unit cell. A spontaneous symmetry-breaking mechanism will, of course, be needed to choose between these two cell-doubled structures. This mechanism can, for instance, arise from the choice of the magnetic easy axis in the system. In Mn_3O_4, this is due to the Mn^{2+} spins. Here, if the easy axis is along the [110] direction, the orbital angle of cell A is $\theta = \pi/2$ and that of cell B is $\theta = -\pi/2$ [see Fig. 7(c)], while for the easy axis being $[1\bar{1}0]$ the orbital angles of the two sublattices are exchanged.

Comparison with experiments performed at low temperature

We will now attempt a comparison of the results obtained from our theoretical analysis thus far with the experimental observations on Mn_3O_4 at low temperatures. The experiments probe the interplay of a magnetoelastic coupling and external magnetic fields on the magnetic and structural ordering of the system [20,22,28]. We begin by recalling that for $T < 32$ K the ordered magnetic state involves a cell-doubled state of distorted tetrahedra (as discussed above). When an external magnetic field is applied along the [100] direction with $T < 32$ K, Nii *et al.* [22] observe a transition to a state with uniformly distorted tetrahedra. This can be understood as follows. The application of the field, $-B_x(S_i^x + S_j^x)$, will naturally mean that spins in the XZ plane will favor alignment along the [100] direction. This ferromagnetic alignment in the XZ plane spins ($\vec{S}_i.\vec{S}_j = +1$) supports a uniform ordering of the orbitals with the orbital angle $\theta = -\pi/2$ in Eq. (16) (see Fig. 4). Further, such uniformly distorted tetrahedra will cause a softening of the acoustic E_g mode [see Eq. (23)], eventually overturning the cell-doubled ground state. Similarly, when the B field is applied along the [010] direction, spin alignment is favored along the y axis [$-B_y(S_i^y + S_j^y)$]. In turn, the ferromagnetic alignment in the YZ planes ($\vec{S}_i.\vec{S}_j = +1$) supports a uniform orbital ordering with $\theta = \pi/2$ (see Fig. 4). Once again, the magnetoelastic coupling ensures that the cell-doubled state will eventually be replaced with a state composed of uniformly distorted tetrahedra. This is again in keeping with the observations of Ref. [22].

The experiments by Kim *et al.* [20,28] show, on the other hand, that for temperatures $32 < T < 42$ K the application of a magnetic field greater than 1 T along the magnetic easy axis (the [110] direction, due to the Mn^{2+} spins) leads to the lattice being distorted from tetragonal to orthorhombic.

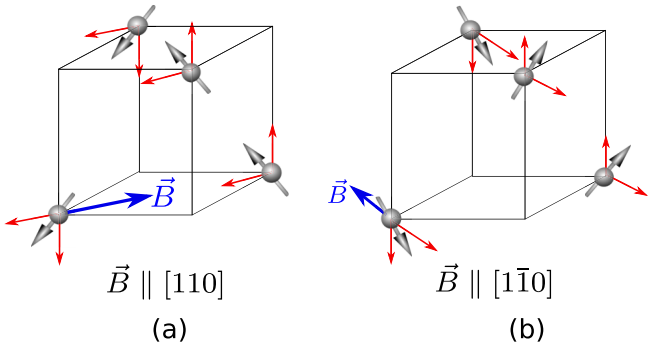

FIG. 8. (a) Application of a magnetic field ($\vec{B}$) along the [110] easy axis enhances the spin-lattice interaction even for $T > 32$ K, and leads to an elongation along the same direction. Red arrows show the spin components along the c and easy axes. (b) Application of a sufficiently large magnetic field along the $[1\bar{1}0]$ direction in the orthorhombically distorted phase below 32 K leads to a rotation of the easy axis towards $[1\bar{1}0]$. The spin-lattice interaction will then lead to an elongation along this direction. Red arrows show the spin components along the c and $[1\bar{1}0]$ directions.

Insight into this finding can again be gained as arising from an increase of the spin-lattice interaction resulting from the applied external magnetic field. The magnetization will now be maximum when the magnetic moments align along the $[\bar{1}\bar{1}0]$ direction. While the Yafet-Kittel configuration involves a canting of the Mn^{3+} spins away from the easy axis ([110]), the application of a sufficiently large external magnetic field along the easy axis will cause them to align along the $[\bar{1}\bar{1}0]$ direction [see Fig. 8(a)]. In turn, this leads to an increased spin-lattice interaction in Eq. (23), resulting in an orthorhombic distortion even for $T > 32$ K.

Further, Kim *et al.* also observe that by applying the magnetic field along the $[1\bar{1}0]$ direction (i.e, a field transverse to the [110] easy axis of the system) for $T < 32$ K a structural transition takes place towards an orthorhombic distortion along the $[1\bar{1}0]$ direction as the applied field is gradually increased. At intermediate values of the transverse field, the system appears to be in a tetragonal phase with a loss of the magnetic ordering. These findings can be understood by noting that the transverse field rotates the choice of the easy axis from its natural direction ([110]) to its perpendicular direction ($[1\bar{1}0]$) [see Fig. 8(b)]. The passage from one to the other will also involve a change from one cell-doubled state of orthorhombically distorted tetrahedra (cell A with orbital angle $\theta = \pi/2$, cell B with $\theta = -\pi/2$) to another in which the orbital angles for the two sublattices are exchanged. As discussed above, both configurations are resultant from the model for the magnetoelastic coupling. Further, at the transition, fluctuations between the two orthorhombic configurations are large and we can expect the outcome to be a tetragonal phase for the system in which the Yafet-Kittel spin order is lost.

V. DISCUSSION AND SUMMARY

We have, in this paper, developed and analyzed a microscopic model for the understanding of orbital and spin ordering in the Mn_3O_4 spinel. Our analysis demonstrates that the qualitative properties of the spinel can be explained by

a spin-orbital Hamiltonian derived by a careful consideration of the 90° nature of the Mn-O-Mn bonding angle, as well as the different electronic energy states of the Mn^{3+} ion. In this way, we realized that the charge-transfer (or Goodenough) SE process is of greater importance than the direct (Anderson) SE for the 90° metal-ligand-metal bond [see, for instance, Eq. (1)]. Upon considering SE interactions together with Jahn-Teller orbital-lattice coupling, we find that interorbital interactions are much stronger than spin-orbital as well as spin-spin interactions. This indicates that orbitals will likely order at energy scales much higher than the spins. Further, the nature of the orbital ordering will influence the nature of the spin ordering.

A consequence of the 90° bonding angle is that the interaction energy between a pair of Mn^{3+} ions is less for similar orbitals ($\theta_i \simeq \theta_j$) than dissimilar orbitals ($\theta_i \simeq \theta_j + \pi$). With this in mind, a variational analysis of our Hamiltonian yields a mixed orbital configuration in the tetragonal phase of the spinel. This mixed ordering of the orbitals then plays an important role in relieving the geometric frustration of spins in a Mn^{3+} tetrahedron. In the tetragonal phase, small values of the effective spin-exchange couplings lead to spins ordering along one-dimensional chains along the [110] and [1$\bar{1}$0] directions, and the experimentally observed three-dimensional Y-K type spin ordering is delayed till very low temperatures. The canted nature of the spins in the Y-K state of Mn^{3+} tetrahedra arises from the competing weak antiferromagnetic Mn^{3+}-Mn^{3+}(J_{BB}) and Mn^{2+}-Mn^{3+}(J_{AB}) spin-exchange couplings. This results in the ferrimagnetic Y-K spin ordering of the Mn_3O_4 spinel system. Further, we have shown that a spin-lattice coupling finally lifts the twofold degeneracy of the Y-K spin configuration via an orthorhombic distortion, leading to a cell-doubled Y-K state. Our model for the spin-lattice interaction is also able to explain the experimentally observed effects of an external magnetic field effect on the Y-K state [20–22,28].

We end by outlining some open directions. Kim *et al.* show that a cell-doubled orthorhombic phase with the magnetic easy axis along the [110] direction can be manipulated using a magnetic field leading to a similar phase with the easy axis along [1$\bar{1}$0], with an intermediate tetragonal phase in which the Y-K spin order is lost [20]. It remains an open question whether such a fluctuation-induced tetragonal phase can be stabilized at yet lower temperatures using, for instance, pressure. As suggested by a recent experiment on the perovskite magnetic insulator $KCuF_3$ [52], a quantum orbital-spin liquid state could potentially be realized in Mn_3O_4. Further, experimental signatures of the mixed nature of the orbital state may be possible to detect in, for instance, x-ray measurements carried out in the low-temperature orthorhombic phase [39]. Finally, in a future work, we will present results on the complete mean field phase diagram of the spin-orbital model derived here, as well as the orbital and spin-excitation spectra in various ordered phases. This should be useful in tracking the passage between competing ground states. It will also be important in quantifying the validity of the classical mixed-orbital variational approach to orbital-spin systems on the spinel lattice.

ACKNOWLEDGMENTS

The authors thank S. Jalal, A. Mukherjee, V. Adak, N. Bhadra, A. Basu, R. Ganesh, G. D. Mukherjee, S. L. Cooper, R. K. Singh, C. Mitra, Y. Sudhakar, and K. Penc for several enlightening discussions. S.P. acknowledges CSIR, Government of India for financial support. S.L. thanks the DST, Government of India for funding through a Ramanujan Fellowship (2010-2015) during which a substantial part of this work was carried out.

APPENDIX

Here we present details of the derivation of the spin-orbital Hamiltonian for the Mn_3O_4 spinel. By considering the fourth-order superexchange mechanism [16], we have four inequivalent sequences of excitation and de-excitation processes for a given intermediate state. We then consider a particular intermediate state by summing over all such equally probable sequences as follows:

$$[XvY] = \tfrac{1}{4}[(X|XvY|X) + (X|XvY|Y) + (Y|XvY|X) + (Y|XvY|Y)], \quad \text{(A1)}$$

where [16]

$$(Z_1|XvY|Z_3) = \frac{t^4 U_v}{\Delta_{Z_1}\Delta_{Z_3}(\Delta_X + \Delta_Y)(\Delta_X + \Delta_Y + U_v)}.$$

$Z_1(Z_3)$ represents the state reached after the first (third) charge-transfer step. $Z_1, Z_2 \in \{X, Y\}$ (for example, see Fig. 2). Then, Eq. (10) can be easily reached from Eq. (A1). We now present the detailed contributions to various SE couplings from the "M", "O", and "N" configurations (in addition to that presented in Sec. II):

$$\begin{aligned}
[M,\uparrow\downarrow;\uparrow\uparrow] &= 2[TtD] + 2[TtS],\\
[M,\uparrow\uparrow;\uparrow\downarrow] &= [TtD] + [TsD] + [TtS] + [TsS],\\
[M,\uparrow\uparrow;\downarrow\downarrow] &= \tfrac{2}{3}([TtD] + [TtS] + [DtD] + [DtS] + [GtD] + [GtS]),\\
[O,\uparrow\uparrow;\downarrow\downarrow] &= [DtD] + 2[DtS] + [StS],\\
[O,\uparrow\downarrow;\downarrow\uparrow] &= \tfrac{1}{2}([DtD] + [DsD] + 2[StD] + 2[SsD] + [StS] + [SsS]),\\
[N,\uparrow\uparrow;\uparrow\uparrow] &= 4[TtT],\\
[N,\uparrow\uparrow;\uparrow\downarrow] &= \tfrac{2}{3}([TtT] + [TsT] + [TtD] + [TsD] + [TtG] + [TsG]),\\
[N,\uparrow\uparrow;\uparrow\downarrow] &= \tfrac{2}{3}([TtT] + [TsT] + [TtD] + [TsD] + [TtG] + [TsG]),
\end{aligned}$$

$$
\begin{aligned}
[N,\uparrow\uparrow;\downarrow\downarrow] &= \tfrac{4}{9}([TtT]+[DtD]+[GtG]+2[TtG]+2[DtG]+2[TtD]),\\
[N,\uparrow\downarrow;\downarrow\uparrow] &= \tfrac{2}{9}([TtT]+[TsT]+[DtD]+[DsD]+[GtG]+[GsG]\\
&\quad +2[TtD]+2[TsD]+2[TtG]+2[TsG]+2[DtG]+2[DsG]),\\
[N,\uparrow\downarrow;\downarrow\downarrow] &= \tfrac{4}{3}([TtT]+[DtT]+[GtT]).
\end{aligned}
\tag{A2}
$$

Using the above equations, one can write the various SE constants (K) in Eq. (8). For the triplet configuration at metal ion sites, this gives $K_L^T = \sum_{\sigma,\sigma'}[L,\uparrow\uparrow;\sigma\sigma']$, while for the singlet configuration we obtain $K_L^S = 2K_L^{\uparrow\downarrow} - K_L^T$, where $\sigma,\sigma' \in \{\uparrow,\downarrow\}$. In obtaining a more compact form of the Hamiltonian (7), one has to put the expression for various projection operators in the expression. The final form of the spin-orbital Hamiltonian is shown in Eq. (11) with SE constants given by

$$
\begin{aligned}
J_\tau &= \tfrac{1}{2}\left(J_O^{\mathcal{O}} - 2J_M^{\mathcal{O}} + J_N^{\mathcal{O}}\right) = \tfrac{1}{18}\big[\big\{9(SS)_+ + 4(GG)_+ + (DD)_+ + 6(DS)_+ + 18\{TG\}_+ + \tfrac{456}{10}[TtT] + \tfrac{184}{10}[TsT]\big\}\\
&\quad - \{12(GS)_+ + 9\{TD\}_+ + 27\{TD\}_+ + 4(GD)_+\}\big],
\end{aligned}
\tag{A3}
$$

$$
\begin{aligned}
J_\sigma &= -\tfrac{1}{2}\left(J_O^{\mathcal{S}} + 2J_M^{\mathcal{S}} + J_N^{\mathcal{S}}\right) = -\tfrac{1}{18}[\{21(DD)_- + 9(SS)_- + 16(TT)_- + 30(DS)_- + 20(DG)_- + 12(GS)_-\}\\
&\quad - \{40(TD)_- + 24(TS)_- + 16(TG)_- + 4(DD) + 4(GG)\}],
\end{aligned}
\tag{A4}
$$

$$
\begin{aligned}
J_\nu &= -\tfrac{1}{2}\left(J_O^{\mathcal{S}} - J_N^{\mathcal{S}}\right) = -\tfrac{1}{18}[\{9(DD)_- + 9(SS)_- + 18(DS)_- + 16(TD)_- + 16(TG)_- - 4(DD) - 4(GG)\}\\
&\quad - \{16(TT)_- + 8(DG)_-\}],
\end{aligned}
\tag{A5}
$$

$$
\begin{aligned}
J_\mu &= -\tfrac{1}{2}\left(J_O^{\mathcal{S}} - 2J_M^{\mathcal{S}} + J_N^{\mathcal{S}}\right) = -\tfrac{1}{18}[\{9(SS)_- + 16(TT)_- + 6(DS)_- + 8(TD)_- + 24(TS)_-\}\\
&\quad - \{3(DD)_- + 4(DG)_- + 12(GS)_- + 16(TG)_- - 4(DD) - 4(GG)\}].
\end{aligned}
\tag{A6}
$$

In these expressions,

$$
[XtY] = \frac{t^4}{4}\frac{\Delta_X+\Delta_Y}{\Delta_X^2\Delta_Y^2}\frac{U_p - J_p}{\Delta_X+\Delta_Y+U_p-J_p}, \tag{A7}
$$

$$
[XsY] = \frac{t^4}{4}\frac{\Delta_X+\Delta_Y}{\Delta_X^2\Delta_Y^2}\frac{U_p + J_p}{\Delta_X+\Delta_Y+U_p+J_p}, \tag{A8}
$$

$[XsY] > [XtY]$, with $X,Y \in \{T,D,S,G\}$. Further,

$$
(XY)_+ = \frac{6}{10}[XtY] + \frac{4}{10}[XsY] = \frac{t^4}{40}\frac{\Delta_X+\Delta_Y}{\Delta_X^2\Delta_Y^2}\left[\frac{6(U_p-J_p)}{\Delta_X+\Delta_Y+U_p-J_p} + \frac{4(U_p+J_p)}{\Delta_X+\Delta_Y+U_p+J_p}\right]. \tag{A9}
$$

As $\Delta_X + \Delta_Y + U_p \gg J_p$, we may write

$$
(XY)_+ = \frac{t^4}{40}\frac{\Delta_X+\Delta_Y}{\Delta_X^2\Delta_Y^2}\frac{(10U_p - 2J_p)}{\Delta_X+\Delta_Y+U_p}. \tag{A10}
$$

As $U_p > J_p$, it can be seen that $(XY)_+ > 0$. Similarly,

$$
(XY)_- = \frac{1}{10}([XtY] - [XsY]) = -\frac{t^4}{20}\frac{\Delta_X+\Delta_Y}{\Delta_X^2\Delta_Y^2}\frac{J_p}{\Delta_X+\Delta_Y+U_p}, \tag{A11}
$$

$$
\{XY\}_+ = \frac{44}{30}[XtY] + \frac{28}{90}[XsY] = \frac{t^4}{360}\frac{\Delta_X+\Delta_Y}{\Delta_X^2\Delta_Y^2}\left[\frac{(160U_p - 104J_p)}{\Delta_X+\Delta_Y+U_p}\right], \quad \& \tag{A12}
$$

$$
(XY) = \frac{1}{10}([XtY] + [XsY]) = \frac{t^4}{20}\frac{\Delta_X+\Delta_Y}{\Delta_X^2\Delta_Y^2}\left[\frac{U_p}{\Delta_X+\Delta_Y+U_p}\right]. \tag{A13}
$$

For the Mn_3O_4 system,

$$
\Delta_T = \Delta - 4J_H, \quad \Delta_D = \Delta + \frac{5}{3}J_H, \quad \Delta_S = \Delta + \frac{13}{3}J_H, \quad \Delta_G = \Delta + J_H, \tag{A14}
$$

and $\Delta = U - J_H$. In the plots of various SE constants shown in Fig. 3, we have employed realistic values of various constants for the Mn_3O_4 spinel taken from the literature [16,31,35,36].

[1] L. Balents, Nature (London) **464**, 199 (2010).
[2] Y. Zhou, K. Kanoda, and T. K. Ng, Rev. Mod. Phys. **89**, 025003 (2017).
[3] M. Fu, T. Imai, T. H. Han, and Y. S. Lee, Science **350**, 655 (2015).
[4] H. A. Jahn and E. Teller, Proc. R. Soc. A **161**, 220 (1937).
[5] I. Bersuker, *The Jahn-Teller Effect* (Cambridge University, Cambridge, England, 2006).
[6] P. Fazekas, *Lecture Notes on Electron Correlation and Magnetism* (World Scientific, Singapore, 1999), Vol. 5.
[7] K. I. Kugel and D. I. Khomskii, Sov. Phys. JETP **37**, 725 (1973).
[8] K. I. Kugel and D. I. Khomskii, Phys. Usp. **25**, 231 (1982).
[9] Y. Yamashita and K. Ueda, Phys. Rev. Lett. **85**, 4960 (2000).
[10] O. Tchernyshyov and G. W. Chern, in *Introduction to Frustrated Magnetism* (Springer, New York, 2011), pp. 269–291.
[11] A. M. Oleś, arXiv:1008.2515.
[12] A. M. Oleś, J. Phys.: Condens. Matter **24**, 313201 (2012).
[13] A. M. Oleś, L. F. Feiner, and J. Zaanen, Phys. Rev. B **61**, 6257 (2000).
[14] D. I. Khomskii, Int. J. Mod. Phys. B **15**, 2665 (2001).
[15] M. V. Mostovoy and D. I. Khomskii, Phys. Rev. Lett. **89**, 227203 (2002).
[16] A. J. W. Reitsma, L. F. Feiner, and A. M. Oleś, New J. Phys. **7**, 121 (2005).
[17] G. B. Jensen and O. V. Nielsen, J. Phys. C **7**, 409 (1974).
[18] B. Chardon and F. Vigneron, J. Magn. Magn. Mater. **58**, 128 (1986).
[19] T. Suzuki and T. Katsufuji, Phys. Rev. B **77**, 220402 (2008).
[20] M. Kim, X. M. Chen, X. Wang, C. S. Nelson, R. Budakian, P. Abbamonte, and S. L. Cooper, Phys. Rev. B **84**, 174424 (2011).
[21] J. H. Chung, K. Hwan Lee, Y. S. Song, T. Suzuki, and T. Katsufuji, J. Phys. Soc. Jpn. **82**, 034707 (2013).
[22] Y. Nii, H. Sagayama, H. Umetsu, N. Abe, K. Taniguchi, and T. Arima, Phys. Rev. B **87**, 195115 (2013).
[23] T. Byrum, S. L. Gleason, A. Thaler, G. J. MacDougall, and S. L. Cooper, Phys. Rev. B **93**, 184418 (2016).
[24] A. Chartier, P. DArco, R. Dovesi, and V. R. Saunders, Phys. Rev. B **60**, 14042 (1999).
[25] L. F. Feiner, A. M. Oleś, and J. Zaanen, Phys. Rev. Lett. **78**, 2799 (1997).
[26] K. Rościszewski and A. M. Oleś, J. Phys.: Condens. Matter **22**, 425601 (2010).
[27] F. Guillou, S. Thota, W. Prellier, J. Kumar, and V. Hardy, Phys. Rev. B **83**, 094423 (2011).
[28] M. Kim, X. M. Chen, Y. I. Joe, E. Fradkin, P. Abbamonte, and S. L. Cooper, Phys. Rev. Lett. **104**, 136402 (2010).
[29] E. Jo, K. An, J. H. Shim, C. Kim, and S. Lee, Phys. Rev. B **84**, 174423 (2011).
[30] R. Tackett, G. Lawes, B. C. Melot, M. Grossman, E. S. Toberer, and R. Seshadri, Phys. Rev. B **76**, 024409 (2007).
[31] L. F. Feiner and A. M. Oleś, Phys. Rev. B **59**, 3295 (1999).
[32] J. Zaanen and G. A. Sawatzky, J. Solid State Chem. **88**, 8 (1990).
[33] R. Englman and B. Halperin, Phys. Rev. B **2**, 75 (1970).
[34] S. Hirai, Y. Goto, Y. Sakai, A. Wakatsuki, Y. Kamihara, and M. Matoba, J. Phys. Soc. Jpn. **84**, 114702 (2015).
[35] A. E. Bocquet, T. Mizokawa, T. Saitoh, H. Namatame, and A. Fujimori, Phys. Rev. B **46**, 3771 (1992).
[36] T. Mizokawa and A. Fujimori, Phys. Rev. B **54**, 5368 (1996).
[37] J. van den Brink and D. I. Khomskii, Phys. Rev. B **63**, 140416(R) (2001).
[38] F. Vernay, K. Penc, P. Fazekas, and F. Mila, Phys. Rev. B **70**, 014428 (2004).
[39] J. C. Lee, S. Yuan, S. Lal, Y. I. Joe, Y. Gan, S. Smadici, K. Finkelstein, Y. Feng, A. Rusydi, P. M. Goldbart *et al.*, Nat. Phys. **8**, 63 (2012).
[40] A. M. Oles, M. Cuoco, and N. B. Perkins, in *Lectures on the Physics of Highly Correlated Electron Systems IV*, edited by F. Mancini, AIP Conference Proceedings Vol. 527 (AIP, New York, 2000), pp. 226–380.
[41] G. Srinivasan and M. S. Seehra, Phys. Rev. B **28**, 1 (1983).
[42] E. Fradkin, *Field Theories of Condensed Matter Physics* (Cambridge University, Cambridge, England, 2013).
[43] Y. Yafet and C. Kittel, Phys. Rev. **87**, 290 (1952).
[44] N. Menyuk, K. Dwight, D. Lyons, and T. A. Kaplan, Phys. Rev. **127**, 1983 (1962).
[45] D. H. Lyons and T. A. Kaplan, Phys. Rev. **120**, 1580 (1960).
[46] M. A. Willard, Y. Nakamura, D. E. Laughlin, and M. E. McHenry, J. Am. Ceram. Soc. **82**, 3342 (1999).
[47] S. L. Gleason, T. Byrum, Y. Gim, A. Thaler, P. Abbamonte, G. J. MacDougall, L. W. Martin, H. D. Zhou, and S. L. Cooper, Phys. Rev. B **89**, 134402 (2014).
[48] M. Matsuda, H. Ueda, A. Kikkawa, Y. Tanaka, K. Katsumata, Y. Narumi, T. Inami, Y. Ueda, and S. H. Lee, Nat. Phys. **3**, 397 (2007).
[49] O. Tchernyshyov, R. Moessner, and S. L. Sondhi, Phys. Rev. B **66**, 064403 (2002).
[50] O. Tchernyshyov, R. Moessner, and S. L. Sondhi, Phys. Rev. Lett. **88**, 067203 (2002).
[51] C. Lacroix, P. Mendels, and F. Mila, *Introduction to Frustrated Magnetism: Materials, Experiments, Theory* (Springer, New York, 2011), Vol. 164.
[52] S. Yuan, M. Kim, J. T. Seeley, J. C. T. Lee, S. Lal, P. Abbamonte, and S. L. Cooper, Phys. Rev. Lett. **109**, 217402 (2012).